Published in final edited form as:
J Biol Chem. 2003 October 17; 278(42): 41114–41125. doi:10.1074/jbc.M306150200.

Structure-Function Analysis of the Bestrophin Family of Anion Channels*

Takashi Tsunenari[‡,§], **Hui Sun**[§,¶,‖], **John Williams**[¶,‖], **Hugh Cahill**[‡], **Philip Smallwood**[¶,‖], **King-Wai Yau**[‡,**,‡‡], and **Jeremy Nathans**[‡,¶,‖,**,§§]

[‡]Department of Neuroscience, The Johns Hopkins University School of Medicine, Baltimore, Maryland 21205

[¶]Department of Molecular Biology and Genetics, The Johns Hopkins University School of Medicine, Baltimore, Maryland 21205

[**]Department of Ophthalmology, The Johns Hopkins University School of Medicine, Baltimore, Maryland 21205

[‖]Howard Hughes Medical Institute, The Johns Hopkins University School of Medicine, Baltimore, Maryland 21205

Abstract

The bestrophins are a newly described family of anion channels unrelated in primary sequence to any previously characterized channel proteins. The human genome codes for four bestrophins, each of which confers a distinctive plasma membrane conductance on transfected 293 cells. Extracellular treatment with methanethiosulfonate ethyltrimethylammonium (MTSET) of a series of substitution mutants that eliminate one or more cysteines from human bestrophin1 demonstrates that cysteine 69 is the single endogenous cysteine responsible for MTSET inhibition of whole-cell current. Cysteines introduced between positions 78–99 and 223–226 are also accessible to external MTSET, with MTSET modification at positions 79, 80, 83, and 90 producing a 2–6-fold increase in whole-cell current. The latter set of four cysteine-substitution mutants define a region that appears to mediate allosteric control of channel activity. Mapping of transmembrane topography by insertion of *N*-linked glycosylation sites and tobacco etch virus protease cleavage sites provides evidence for cytosolic N and C termini and an unexpected transmembrane topography with at least three extracellular loops that include positions 60–63, 212–227, and 261–267. These experiments provide the first structural analysis of the bestrophin channel family.

Chloride channels play diverse roles in both excitable and nonexcitable cells (1–3). At the plasma membrane of nerve and muscle, they stabilize the resting potential and inhibit electrical excitability. In epithelia, they play essential roles in fluid and electrolyte transport. Another role for chloride channels is seen in the acidification of intracellular organelles such as endosomes. To maintain electrical neutrality, the inward pumping of protons must be accompanied by a chloride current (4). A variation on this theme appears to underlie the essential role of chloride channels in the extreme acid response of enteric bacteria (5),

*This work was supported by the Howard Hughes Medical Institute and the NEI, National Institutes of Health. The costs of publication of this article were defrayed in part by the payment of page charges. This article must therefore be hereby marked "*advertisement*" in accordance with 18 U.S.C. Section 1734 solely to indicate this fact.

[‡‡]To whom correspondence may be addressed. kwyau@mail.jhmi.edu. [§§]To whom correspondence may be addressed. jnathans@jhmi.edu.

[§]Both authors contributed equally to this work.

suggesting that one of the original roles of chloride channels may have been in promoting microbial survival at low pH.

Over the past 25 years, three distinct families of chloride channels have been molecularly characterized: the ClC family, the ligand-gated chloride channels of the γ-aminobutyric acid/glycine receptor family, and the cystic fibrosis transmembrane conductance regulator. In mammals there are nine members of the ClC family, and these function as dimers with a complex transmembrane topography (6). The glycine and γ-aminobutyric acid receptor gene families are composed, respectively, of 5 and at least 15 homologous subunits (7,8), and within each family the subunits coassemble to form pentameric ligand-gated chloride channels. Cystic fibrosis transmembrane conductance regulator is distinctive in being the only ATP-binding cassette transporter that is also a channel; its expression is mostly in epithelia (9). A fourth type of chloride channel, corresponding to a chloride conductance in tracheal epithelium, has been described (10,11), but its identity remains controversial. At present, the extent to which the known chloride channel families account for the diversity of observed chloride conductances remains an open question.

The most recent additions to the list of molecularly defined chloride channels are the bestrophins. Bestrophins were originally defined as a family of over 20 related sequences in the *Caenorhabditis elegans* genome with no homology to any proteins of known function. The first mammalian bestrophin was identified as the protein product of the gene responsible for autosomal dominant vitelliform macular dystrophy (VMD),[1] also known as Best disease (12, 13). VMD is characterized by the following symptoms: (*a*) a diminution or loss of the late light peak of the electro-oculogram, caused by a defect within the retinal pigment epithelium (RPE); (*b*) a progressive loss of central vision; and (*c*) an accumulation of debris within and beneath the RPE (14–20). In keeping with the localization of these defects, bestrophin mRNA and protein are highly enriched in the RPE (12,13,21).

Evidence that the bestrophins function as chloride channels comes from their expression in transfected 293 cells (22). These experiments demonstrate the following: (*a*) each of four different bestrophin family members, two from human, one from *Drosophila*, and one from *C. elegans*, produces a chloride conductance with a distinct I-V relationship and/or ion selectivity; (*b*) the chloride current conferred by wild type human bestrophin (hBest1) is rapidly inactivated by sulfhydryl-reactive agents, whereas the current conferred by a cysteine-less hBest1 is resistant to such inactivation; (*c*) the bestrophins oligomerize to form tetramers or pentamers; (*d*) the chloride conductance observed upon expression of hBest1 is calcium-sensitive; and (*e*) multiple hBest1 mutants responsible for VMD dominantly inhibit the chloride conductance associated with wild type hBest1, consistent with their dominance *in vivo*. The most straightforward interpretation of these diverse observations is that the bestrophins function directly as chloride channels, although they do not exclude the possibility that the bestrophins may coassemble with additional subunits in the RPE or in 293 cells.

In the present paper we report the primary sequence and functional expression of the remaining two members of the human bestrophin family, an analysis of the functional and transmembrane topographies of hBest1 using cysteine-substitution mutagenesis and whole-cell recording, and a map of the transmembrane topography of hBest1 using insertional mutagenesis of *N*-glycosylation and protease cleavage sites. These data reveal an intriguing pattern of allosteric channel regulation and an unusual transmembrane disposition for the bestrophins. They also

[1]The abbreviations used are: VMD, vitelliform macular dystrophy; MTSEA, 2-aminoethylmethane thiosulfonate; MTSET, methanethiosulfonate ethyltrimethylammonium; RPE, retinal pigment epithelium; TEVP, tobacco etch virus protease; ER, endoplasmic reticulum; mAb, monoclonal antibody; hBestl, human bestrophinl; EGFP, enhanced green fluorescent protein; PBS, phosphate-buffered saline; hGH, human growth hormone.

lend further support to the conclusion that the bestrophins function as *bona fide* chloride channels.

EXPERIMENTAL PROCEDURES

Amplification and Cloning of Bestrophin cDNAs

PCR amplification was performed using putative coding region and 3′-untranslated region primers based on the hBest3 and hBest4 genomic sequences. Human testis, fetal brain cDNA, and DNA prepared from a human retina cDNA library (23) were used as templates. PCR products were cloned, sequenced, assembled to reconstruct the complete coding regions, engineered to carry an optimal translation initiation sequence (CCAC-CATG) upstream of the initiator methionine, and inserted into mammalian expression vector pRK5.

Site-directed Mutagenesis

Mutations were constructed in an hBest1 variant carrying a C-terminal Rim3F4 epitope tag (22,24). Site-directed mutagenesis was performed by PCR amplification, and all DNA segments that were amplified by PCR were sequenced to confirm the desired mutation and to rule out spurious ones.

Mapping of Transmembrane Topography by N-Glycosylation

293 cells were transiently transfected using FuGENE 6 (Roche Applied Science), harvested 24 h later by detachment in 1× PBS and 5 mM EDTA, and pelleted at 3,000 × *g* for 5 min in a microcentrifuge. The cell pellet from one well of a 6-well plate was dissolved in 100 μl of solubilization buffer (1% Triton X-100, 1× PBS, 10% glycerol, 0.1 mM phenylmethylsulfonyl fluoride, and chymostatin, leupeptin, antipain, and pepstatin A, each at 1 mg/ml). After incubating on ice for 30 min, insoluble material was removed by centrifugation at 15,000 × *g* in a microcentrifuge at 4 °C for 30 min. 10 μl of supernatant was mixed with 40 μl of solubilization buffer with or without 125 units of peptide: *N*-glycosidase F (New England Biolabs, Beverly, MA). After 1 h of incubation at room temperature, the reaction was stopped by addition of an equal volume of 2× SDS sample buffer and analyzed by immunoblotting with mAb Rim3F4.

Mapping of Transmembrane Topography by Tobacco Etch Virus Protease (TEVP) Cleavage

TEVP, tagged with 6 histidines, was expressed in *Escherichia coli*, denatured in urea, purified by metal chelate chromatography to apparent homogeneity, and refolded by dialysis, essentially as described (25). 293 cells were transiently transfected with hBest1 expression plasmids and harvested as described above. The cell pellet from 1 well of a 6-well plate was resuspended in 100 μl of cold TEVP buffer (50 mM Tris-HCl, pH 8.0, 10 mM dithiothreitol, and 5 mM EDTA). Cells were broken using a small motor-driven homogenizer for 1 min, and nuclei were removed by centrifugation in a microcentrifuge at 600 × *g* rpm for 5 min at 4 °C. 10 μl of the supernatant was added to 40 μl of TEVP buffer without TEVP, with 1 μg of TEVP, or with 1 μg of TEVP and 1% Triton X-100. After 3 h of incubation at 30 °C, an equal volume of 2× SDS loading buffer was added to stop the reaction. TEVP cleavage was monitored by immunoblotting as described above. The human growth hormone (hGH)-TEVP site-Myc epitope-human epidermal growth factor receptor3 extracellular domain (HER3EC) fusion protein was constructed by inserting a Myc epitope between the TEVP site and a HER3EC coding region that had been inserted into the mammalian expression vector pSVGH-0 (26). For experiments with this hGH fusion protein, the secreted protein was removed from the medium by washing the transfected cells with serum-free medium prior to harvesting.

Whole-cell Recordings

293 cells were transfected with a bestrophin expression plasmid mixed with an EGFP plasmid at a 10:1 ratio by using FuGENE 6 (Roche Applied Science) at 2 μg of DNA per 3.5-cm plate. The EGFP plasmid alone (2 μg) was used as a transfection control. Approximately 24 h after transfection, the cells were detached from the plates with 5 mM EDTA in 1× PBS and were replated at lower density. Approximately 60 h after transfection, whole-cell recordings were performed at room temperature (22–25 °C) on single, isolated green cells identified under an inverted fluorescence microscope. Isolated cells were chosen because electrical coupling between adjacent cells would otherwise lead to space-clamp problems and incomplete dialysis of the coupled cell interior with the pipette solution. Standard extracellular solution contained (in millimolar): 140 NaCl, 5 KCl, 2 $CaCl_2$, 1 $MgCl_2$, 10 glucose, and 10 Na-Hepes, pH 7.4. Standard pipette solution contained (in millimolar): 148 CsCl, 2 $MgCl_2$, 0.5 $CaCl_2$, 2 EGTA, and 10 Na-Hepes, pH 7.3, giving 40 nM free [Ca^{2+}]. CsCl was chosen to block endogenous K^+ currents. In some of the sulfhydryl modification experiments, 20 mM cysteine was added to the pipette solution in order to test the effect of intracellular cysteine. In this case, the pipette solution contained (in millimolar): 20 cysteine, 128 CsCl, 2 $MgCl_2$, 0.5 $CaCl_2$, 2 EGTA, and 10 Na-Hepes, pH 7.3.

Xenopus Oocyte Recordings

Xenopus laevis oocytes were obtained surgically under anesthesia in 0.3% tricaine methanesulfonate solution. After enzymatic treatment for defolliculation (2 mg/ml collagenase type I (Sigma), 2–3 h at room temperature in modified Barth's saline (88 mM NaCl, 1 mM KCl, 2.4 mM $NaHCO_3$, 0.33 mM $Ca(NO_3)_2$, 0.41 mM $CaCl_2$, 0.82 mM $MgSO_4$, 15 mM Hepes, pH 7.6, supplemented with 10 units/ml penicillin and 10 μg/ml streptomycin)), stage V–VI oocytes were selected and maintained for 1 day in modified Barth's saline at 17 °C before cRNA injection (50 nl/oocyte) using a Nanoject microinjecttor (Drummond Scientific, Broomall, PA). Whole-cell currents of oocytes were measured within 1–5 days after injection using a standard two-electrode voltage clamp amplifier (OC-725, Warner Instruments, Hamden, CT) with micropipettes of 0.5–3-megohm resistance filled with 3 M KCl. The recordings were performed in solution containing 96 mM NaCl, 2 mM KCl, 1.8 mM $CaCl_2$, 1 mM $MgCl_2$, 5 mM Hepes, pH 7.4. Current and voltage data were acquired and analyzed with DIGIDATA 1321A and pClamp 8 software (Axon Instruments, Union City, CA).

Sulfhydryl Modification

After establishment of a stable whole-cell recording, 2-trimethylammonioethylmethanethiosulfonate (MTSET) as the bromide salt (Toronto Research Chemicals, Ontario, Canada) in standard extracellular solution was added to the recording chamber in place of the standard solution. For these experiments, a 0.1 M MTSET stock solution was prepared in distilled water, stored on ice, and used within 90 min. The standard extracellular solution with MTSET diluted to the indicated working concentration was made immediately prior to use.

RESULTS

Identification of Four Bestrophin Family Members in the Human Genome

Homology searches of the nearly complete human genome sequence revealed four sequences with high homology to human bestrophin. One of these corresponds to bestrophin itself, referred to here as hBest1. A second sequence corresponds to hBest2, a bestrophin family member that was functionally characterized by Sun *et al.* (22). The remaining two sequences, referred to here as hBest3 and hBest4, are divided into putative introns and exons in a manner that closely resembles the gene organization of hBest1. Transcripts derived from hBest3 and

hBest4 appear to be rare in the major human tissues, as they were undetectable by hybridization to RNA blots of adrenal, brain, heart, kidney, liver, lung, pancreas, retina, skeletal muscle, testis, fibroblasts, and white blood cells (data not shown). Consistent with this observation, hBest3 and hBest4 were represented in the November, 2002, EST data base by only 18 and 4 entries, respectively, out of a total of 4.9 million human EST entries. Stohr *et al.* (27) have recently reported the existence of the hBest3 and hBest4 sequences in the human genome data base and have identified transcripts from hBest3 and hBest4 in a variety of tissues by reverse transcriptase-PCR.

To verify the predicted intron-exon structure of the hBest3 and hBest4 genes and to obtain cDNA sequences suitable for functional expression in transfected cells, the coding regions of hBest3 and hBest4 were assembled by a combination of reverse transcriptase-PCR and library screening of cDNA from human testis and retina (hBest3) or human testis and fetal brain (hBest4; Fig. 1). The resulting cDNA sequences show hBest3 and hBest4 to be 668 and 474 amino acids in length, respectively. The cDNA sequences also confirm the intron-exon structures predicted from the hBest1 homology search of the human genome. In pairwise comparisons, the four human bestrophins share between 56 and 66% sequence identity within the conserved N-terminal ~360 amino acids but show minimal homology within the C-terminal domain (Table I).

Evolution of the Bestrophin Family

Homology searches of the nearly complete mouse and pufferfish (*Fugu rubripes*) genome sequences reveal four and three bestrophin homologues, respectively. Among the currently complete invertebrate genomes, 4 bestrophins are found in *Drosophila melanogaster*, 2 in mosquito (*Aenopheles gambia*), and 25 in *Caenorhabditis elegans*. As noted above in the context of the human sequences, bestrophins in all of these species are divided into a conserved N-terminal domain that includes the putative transmembrane regions, and a C-terminal domain that is highly variable in both length and sequence (Table I). Based on this differential conservation, we have assigned position 364 in hBest1 as the border between the N- and C-terminal domains.

In comparing the four pairs of human and mouse bestrophin orthologues, the N- and C-terminal domains show 69–95 and 34–74% identity, respectively (Table I). In pairwise comparisons among all non-orthologous human and mouse bestrophins, the N- and C-terminal domains show 44–67 and 4–19% identity, respectively (Table I). Fig. 1*B* shows an unrooted dendrogram depicting the amino acid sequence divergence among human, mouse, and pufferfish N-terminal domains. In comparing N-terminal domain sequences among mouse and human orthologues, Best2 and Best3 are nearly identical, whereas Best1 and Best4 show considerably greater divergence. Similar analyses with both vertebrate and invertebrate bestrophin N-terminal domains place most of the vertebrate bestrophins on a separate and relatively conserved branch within the larger bestrophin family. Interestingly, almost all of the VMD-associated mutations reported to date are single amino acid substitutions that cluster within the N-terminal domain (28–31). However, within this domain these mutations show only modest colocalization with evolutionarily conserved positions (Fig. 1*C*).

Functional Properties of hBest3 and hBest4

To determine whether hBest3 and hBest4 can function as chloride channels, as has been shown for hBest1 and hBest2, each was expressed together with enhanced green fluorescent protein (EGFP) in transiently transfected 293 cells, as described (22). In whole-cell recordings, hBest3 and hBest4 transfected cells each exhibited a distinctive conductance that was not observed in control cells transfected with EGFP alone (Fig. 2). In Fig. 2, the mean whole-cell currents 1 day after transient transfection were 1831 ± 501 pA (n = 5 cells) for hBest3 and 1248 ± 788

pA (n = 4 cells) for hBest4 when measured 5 s (hBest3) or 320 ms (hBest4) after stepping from 0 to −150 mV. However, considerably larger whole-cell currents are typically seen for cells transfected with hBest4; indeed, for many of these cells the currents were too large to permit reliable whole-cell measurements. As seen in Fig. 2, the I-V relation of hBest4 resembles that seen for hBest1, whereas the I-V relation of hBest3 is the most strongly rectifying of any bestrophin tested thus far.

Cells expressing hBest3 or hBest4 exhibit a characteristic time course of whole-cell current in response to a negative voltage step (Fig. 2). Cells expressing hBest3 respond with a prolonged and steady increase in conductance that continues for at least 20 s. The measured time constant of this current increase is 9.4 ± 0.8 s (n = 3 cells). When hBest3-expressing cells are returned from −150 to −50 mV, they exhibit a slow tail current. Cells expressing hBest4 respond to a negative voltage step with a rapid and roughly linear current response which then decreases by ~20% over the ensuing several hundred milliseconds. In earlier work, we observed that cells expressing hBest1, hBest2, and the *Drosophila* bestrophin dmBest1 show minimal changes in current amplitude during a 320-ms voltage step, and that cells expressing the *C. elegans* bestrophin ceBest1 show little time dependence of the current response except at large negative voltages (22). Taken together, these data point to hBest3 as the most atypical of the four human bestrophins.

In preliminary experiments aimed at exploring alternate expression systems for the bestrophins, we were unable to detect new chloride currents in *Xenopus* oocytes following injection of synthetic hBest1 mRNA, whereas control injections of ClC-0 mRNA with identical 5′- and 3′-untranslated regions produced large chloride currents. These data suggest that 293 cells may contain chaperones, trafficking proteins, and/or channel subunits that are required for bestrophin function or plasma membrane localization.

Identification of Cys-69 as the Principal Target for Wild Type hBest1 Channel Modification by MTSET

In earlier work, we observed that cells expressing hBest1 exhibit a rapid loss of whole-cell current upon exposure to the cysteine modification reagent 2-aminoethylmethane thiosulfonate (MTSEA), whereas cells expressing an hBest1 mutant in which all five cysteines were simultaneously mutated to alanine are resistant to inactivation by MTSEA (22). Inactivation by MTSEA almost certainly involves covalent modification of one or more cysteines that are accessible to the extracellular space because exposure to MTSET, a cysteine modification reagent with a fixed positive charge and therefore even greater membrane impermeability, produces nearly identical kinetics of inactivation (Fig. 3*A*; compare with Fig. 3 of Ref. 22).

To determine which cysteine(s) within hBest1 are responsible for inactivation, we determined the effect of MTSET exposure on five hBest1 mutants, each of which retains only one of the five cysteines. These five hBest1 mutants, referred to as “C23-retained,” “C42-retained,” “C69-retained,” “C221-retained,” and “C251-retained,” carry alanines in place of the remaining four cysteines. Importantly, none of the five cysteines is conserved across the bestrophin family, indicating that they are unlikely to be involved in disulfide bonds. As seen in Fig. 3, *B* and *C*, each of the five single cysteine mutants confers a readily measurable whole-cell current, but only C69-retained is inactivated by MTSET. The importance of Cys-69 in conferring sensitivity to MTSET is further strengthened by the observation that mutating this residue to alanine (C69A) in the context of an otherwise wild type hBest1 sequence results in resistance to MTSET-dependent inactivation (Fig. 3*B*). These data place Cys-69 in or accessible to the extracellular space and indicate that covalent modification of Cys-69 with the bulky and positively charged trimethyl adduct derived from MTSET either blocks the channel pore directly or induces an allosteric transition that results in channel closure.

Channel Activation and Inhibition by MTSET following Cysteine-substitution Mutagenesis

Covalent modification of cysteines that have been introduced by site-directed mutagenesis is a widely used method for mapping the functional and transmembrane topography of ion channels (32). As described below, we have used this approach to explore the accessibility of different sites in hBest1 to covalent modification and to determine the consequences of such modification on channel activity. In these experiments, we have used the C69A mutant rather than the cysteineless mutant as the starting point for further mutagenesis because the C69A mutant represents the minimal sequence alteration that confers resistance to MTSET-dependent inactivation. Moreover, although both mutants confer roughly wild type levels of whole-cell current, currents produced by the cysteine-less mutant are, on average, less stable.

An initial set of cysteine-substitution mutants was constructed with the aim of identifying one or more positions that, when mutated to cysteine, would both produce functional channels and exhibit an MTSET-dependent change in whole-cell current. With this goal in mind, the choice of mutations was guided by the following considerations. First, positions where VMD-associated amino acid substitutions introduce either lysine or arginine were targeted because covalently modifying a preassembled channel with the positively charged MTSET might be expected to mimic the effect of substitution with either of these amino acids. Second, positions where cysteines are found in other bestrophin family members were targeted on the assumption that the native channel would be more likely to tolerate the introduction of a cysteine at these positions. Third, hydrophilic residues within the four most prominent hydrophobic segments, as defined by the hydropathy plot in Fig. 8, were targeted on the assumption that one or more of these might be part of or near the channel pore. Fourth, nonconserved polar residues immediately adjacent to putative transmembrane domains were targeted as potentially accessible to MTSET in the aqueous environment and near the mouth of the channel pore. Finally, residues near Cys-69 were targeted because of the known susceptibility of this position to MTSET modification.

We also constructed a second set of cysteine substitutions to test the MTSET susceptibility of each position in the putative second transmembrane domain and to examine positions near those in the first set of substitutions that had conferred MT-SET susceptibility. In interpreting these cysteine substitution experiments, we note that there is a formal possibility that one or more of the endogenous cysteines that remain in the C69A background (at positions 23, 42, 221, and 251) could be induced to react with MTSET as a result of structural perturbations induced by the newly introduced cysteine.

Altogether, 41 cysteine substitution mutants were examined. Substitutions at positions 27, 75, 76, 77, 81 82, 85, 88, 89, 91, 92, 96, 135, 143, 224, and 237 failed to give detectable whole-cell currents under our standard recording conditions and were not studied further. Substitutions at positions 12, 16, 60, 71, 74, 86, 95, 108, 133, 169, 185, 225, 231, 268, and 293 produced readily measurable whole-cell currents that appear to be completely or largely unaffected by exposure to MTSET. Each of the remaining 10 cysteine-substitution mutants produced measurable whole-cell currents that showed one of several responses to applied MTSET as follows: a large sustained activation (positions 79, 80, 83, and 90); a large sustained inhibition (position 226); a small sustained activation (position 87); a small sustained inhibition (position 78); or a transient activation followed by inhibition (positions 84, 99, and 223). In this context, large and small are defined as greater and less than 2-fold, respectively. Examples of these current responses are seen in Fig. 4.

Fig. 4 shows that the large MTSET-induced activation of C69A/V90C and the large MTSET-induced inhibition of C69A/A226C are insensitive to the inclusion of 20 m_M cysteine in the recording pipette, whereas the MTSET-induced inactivation of C69A/N99C is eliminated when 20 m_M cysteine is included in the pipette. As MTSET is largely membrane-impermeant,

any quenching of MTSET modification in these experiments should arise from encounters between intracellular cysteine and extracellular MTSET molecules. Therefore, this result suggests that position 99 is accessible to small hydrophilic molecules applied to either side of the plasma membrane. In the absence of a three-dimensional structure for the bestrophins, the structural basis for this dual accessibility is unclear.

Several cysteine-substitution mutants show a biphasic response to MTSET. Although the molecular mechanism of the biphasic response is at present unclear, we can envision the following three general explanations: (*a*) it could represent a pair of allosteric transitions, one rapid and one slow, that are induced by the same covalent modification event but have opposite effects on channel function; (*b*) it could arise from MTSET modification of different numbers of subunits in a multimeric hBest1 channel; or (*c*), as noted above, if the introduced cysteine induced one or more of the four endogenous cysteines to react with MTSET or to differentially alter channel conductance upon its reaction with MTSET, a biphasic response could reflect differential rates of modification of different cysteines. In the C69A/N99C mutant shown in Fig. 4, the selective elimination of the second (inhibitory) phase by application of intracellular cysteine from the recording pipette implies that each channel possesses more than one MTSET reaction target, and therefore argues against the first of the three possibilities.

Several interesting patterns have emerged from the cysteine substitution experiments. First, as noted above, cysteine substitution at five positions produces a sustained increase in membrane current. For four of these, the increase is greater than 2-fold, and for one, C69A/V90C, it averages 5-fold. These data suggest that in transfected 293 cells hBest1 channels are normally maintained in a partially inhibited state and that they are poised to undergo an activating allosteric transition. Second, when the 18 cysteine-substitution mutants in the second putative transmembrane domain are arrayed on a helical wheel diagram, the five mutants that show sustained activation are found to cluster along one side (Fig. 4*B*). The only position in this region that shows an MTSET effect and does not lie along this face of the helical wheel is Ile-78. These data support an α-helical model for this region and specifically suggest that modifications of this helix are coupled to an activating allosteric transition. Finally, the MTSET sensitivity of cysteine-substitution mutants at positions 99, 223, and 226 are at odds with the simplest transmembrane model for hBest1 based on the hydropathy profile (*e.g.* Ref. 28), which assigns positions 95–225 to a single large intracellular loop. Within this region, we observe small biphasic MTSET effects with C69A/N99C and C69A/H223C and a large monophasic MTSET-dependent inhibition of C69A/A226C. The rapid (time constant = 20 s) and nearly complete (~80%) inhibition seen for C69A/A226C in the presence of 1 m_M MTSET suggests that this position is readily accessible to externally applied MTSET (Fig. 4*A*). By way of comparison, Cys-69, which is very likely to face the extracellular space (see below), reacts with a time constant of 100 s in the context of an otherwise wild type bestrophin sequence, and with a time constant of 23 s in the absence of the other four endogenous cysteines (Fig. 3, *A* and *B*). The simplest interpretation of these data is that position 226 also resides on the extracellular face of the protein.

Mapping Transmembrane Topography by Insertional Mutagenesis

To define systematically the transmembrane topography of hBest1, we employed two complementary approaches based on insertional mutagenesis. In the first approach, consensus *N*-linked glycosylation sites were inserted at 25 locations within hBest1 to determine which regions face the lumen of the endoplasmic reticulum (ER) as determined by their accessibility to the glycosyltransferase on the inner face of the ER membrane. These mutants are named according to the codon immediately preceding the insertion, *e.g.* hBest1-GI-165 refers to the insertion of the amino acid sequence GGNATGG, containing an Asn-*X*-Thr consensus glycosylation site, immediately after codon 165.

The second approach builds on work by others (33) showing that mechanical disruption of mammalian cells produces membrane vesicles from intracellular membranes that are largely oriented with their cytosolic surfaces facing outward, leading to the selective accessibility of the cytosolic domains of integral membrane proteins in these vesicles to cleavage by added proteases. To map sites of protease accessibility, consensus cleavage sites for the tobacco etch virus protease (34) were inserted at 22 locations within hBest1, and the mutant proteins were then incubated with TEVP in cellular homogenates either in the presence or absence of detergent. For the TEVP site insertions, the naming system is analogous to that described above for *N*-glycosylation insertions, *e.g.* hBest1-TI-165 refers to the insertion of the amino acid sequence GGENLYFQGGG, containing the consensus TEVP site EXXYXQ(S/G), immediately after codon 165. In both strategies, the insertions were targeted to regions of hBest1 enriched in charged and polar amino acids to increase the probability that the insertion would reside at the surface of the folded protein. Flanking glycines were included to improve accessibility to the glycosyltransferase or to TEVP. We note that, in analyzing these insertion mutants, we have not attempted to systematically assess protein function by measuring whole-cell currents in transfected cells. Whereas the roughly equivalent yield of the different insertion mutants suggests that in each case the bulk of the protein is correctly folded, the possibility exists that some fraction of the protein in one or more of the mutants may be incorrectly folded.

Insertion of N-Glycosylation Sites

The *1st 3 panels* in Fig. 5 show the electrophoretic mobilities of an initial set of 18 glycosylation site insertion mutants at 16 locations, and the *last 2 panels* show the electrophoretic mobilities of a second set of 9 mutants designed to more finely probe the interval between codons 118 and 228. When produced in 293 cells, wild type hBest1 appears not to be modified by *N*-linked glycosylation as judged by the failure of endoglycosidase F treatment to alter its electrophoretic mobility in SDS-PAGE (Fig. 5). As a consequence, wild type hBest1 tagged with the Rim3F4 epitope migrates as a sharp band of ~70 kDa thus permitting the clear identification of derivatives with the ~3-kDa increase in molecular mass expected for the addition of a single *N*-linked oligosaccharide chain. As seen in Fig. 5, *N*-glycosylation insertions after positions 60, 63, 212, 218, 223, 227, 261, 264, and 267 show a second band of ~3 kDa higher molecular mass, and in each case, this band is eliminated by treatment with endoglycosidase F. These positions are therefore assigned to the luminal or outer face of the protein.

For those insertion mutants that show *N*-glycosylation, none are modified with an efficiency greater than 50%. This relatively low efficiency may be related to the accessibility of the inserted *N*-linked glycosylation sites. Consistent with this idea, we observe increased glycosylation efficiency if the inserted *N*-glycosylation site is flanked by four or five rather than two amino acids, as seen in comparing the insertion of GGNATGG with SGSGNATGSGS or GGNATNATGG after position 264 (the latter two are indicated in Fig. 5 with *single* and *double asterisks*, respectively). Popov *et al.* (35) have shown that an *N*-glycosylation site must reside at least 12–14 amino acids from the membrane for efficient *N*-glycosylation (but see Ref. [36] for a dissenting view). As described more fully below (and illustrated in Fig. 8), the hydropathy profile of hBest1 predicts that transmembrane segments are likely to flank hydrophilic segments between amino acids ~55–75 and ~255–270. If these two hydrophilic segments face the ER lumen, as the *N*-glycosylation data suggest, then insertions at amino acids 60, 63, 261, 264, and 267 might be inefficiently glycosylated as a result of their close proximity to the membrane. As noted by others, these considerations emphasize one limitation of topography mapping using insertion of *N*-glycosylation sites; a failure to observe *N*-glycosylation of the insert should not be interpreted as evidence for cytosolic localization (33,35,37).

Insertion of TEVP Cleavage Sites

All of the hBest1 protein produced in 293 cells appears to be membrane-associated, and the vast majority accumulates within intracellular membranes (Fig. 6). To control for the integrity and sidedness of intracellular membrane vesicles obtained by mechanical disruption, 293 cells were transfected with an efficiently secreted fusion protein in which hGH was linked via a TEVP cleavage site to a Myc epitope-tagged human epidermal growth factor receptor 3 extracellular domain (HER3EC; Fig. 7*A*). The hGH-TEV-myc-HER3EC fusion protein serves as a reporter for the luminal space within the secretory pathway. As expected, this fusion protein is resistant to TEVP cleavage in the absence of detergent, but is susceptible to TEVP cleavage in the presence of 1% Triton X-100 (Fig. 7*A*), confirming earlier reports that cell lysis by mechanical disruption efficiently produces sealed vesicles oriented with their cytosolic faces outward (*e.g.* Ref. 33). This fusion protein appears to be an especially efficient substrate for TEVP cleavage, most likely because the cleavage site is located between a polyhistidine tract and the Myc epitope, both of which are likely to be unstructured.

Fig. 7*B* shows the results of TEVP cleavage of 18 TEVP site insertion mutants at 17 locations in the absence or presence of 1% Triton X-100. Most TEVP site insertions in hBest1 show no detectable cleavage either in the presence or absence of Triton X-100 (Fig. 7*B*). These insertions should be considered uninformative, because failure to observe TEVP cleavage in the presence of detergent most likely reflects either poor accessibility or an inappropriate conformation of the TEVP cleavage site. Highly efficient cleavage is only seen for insertions after positions 355, 416, and 498, and for these mutants cleavage efficiency is not significantly affected by detergent addition. These data indicate that the C-terminal domain of hBest1 faces the cytosol. Lower efficiency TEVP cleavage was observed for insertions after positions 154 and 323, and this efficiency was either unaffected (TI-154) or modestly inhibited (TI-323) by 1% Triton X-100, suggesting that these sites also face the cytosol. Insertions after positions 63 and 261 also show lower efficiency TEVP cleavage, but with the property that the cleavage efficiency is enhanced in the presence of 1% Triton X-100, suggesting that these positions face the lumen of the ER. Insertions after positions 56 and 60 shows very inefficient and detergent-independent cleavage, which could be interpreted as evidence for a cytosolic location for these positions. However, the *N*-glycosylation data places positions 60 and 63 in the ER lumen, and the detergent enhancement of cleavage at position 63 further supports that assignment. Therefore, we attribute low level cleavage at positions 56 and 60 to misfolded protein.

At positions 10 and 14, TEVP cleavage would result in mobility shifts of only ~1–2 kDa, at the resolution limit of SDS-PAGE. To examine this region more rigorously for cleavage, insertions of a triple Myc epitope followed by a TEVP cleavage site were constructed at these two locations. The predicted ~6-kDa mobility shift produced by TEVP cleavage was readily detected independent of detergent addition for this larger insertion after position 10 (Fig. 7*B*), indicating that this region faces the cytosol; a lower level of detergent-independent cleavage was also observed for insertion after position 14 (data not shown). An additional five TEVP cleavage site insertions at positions 105, 118, 218, 223, and 227 were tested, and these showed either no detectable cleavage or very low levels of TEVP cleavage independent of detergent (data not shown).

In summary, the analysis of *N* -glycosylation site insertions and TEVP cleavage site insertions places segments 60–63, 212–227, and 261–267 on the luminal face of the ER (and therefore topologically outside the cell), and the extreme N terminus and the region C-terminal to position 355 in the cytosol. The TEVP cleavage data are also suggestive of a cytosolic location for positions 154 and 323.

DISCUSSION

Evolution and Functional Diversity in the Bestrophin Family

The most striking feature of any alignment of bestrophin family members, whether orthologues or paralogues, is the relatively high conservation of the N-terminal ~360 amino acids and the relatively low conservation of the remaining 100–300 C-terminal amino acids. As the N-terminal domain includes all of the putative membrane-spanning regions, it seems likely that those parts of the protein that are most intimately associated with the channel reside within this domain. The evidence reported here localizing the largely hydrophilic C terminus to the cytosol suggests that the C-terminal domain may anchor the bestrophins to cytoskeletal proteins or serve a modulatory role, as seen for example with cytoplasmic β subunits of potassium channels (38). In this regard, it is interesting that porcine Best1 has been reported recently to associate with protein phosphatase 2A, and recombinant human bestrophin can serve as a substrate for protein phosphatase 2A-dependent dephosphorylation (39).

In comparing the six bestrophins for which whole-cell currents have been measured (four from human, one from *Drosophila*, and one from *C. elegans*; Ref. [22] and the present work), several properties are observed to vary among them, as follows. (*a*) The I-V relation is nearly linear for hBest2 and hBest4, weakly rectifying for hBest1, moderately outward rectifying for dmBest1, moderately inward rectifying for ceBest1, and strongly inward rectifying for hBest3. (*b*) The time course of the whole-cell response to a negative voltage step is rapid for hBest1, hBest2, and dmBest1, with no evidence for a second slower component. ceBest1 and hBest4 show a rapid component, followed by a slow increase in current for ceBest1 and a slow decrease in current for hBest4. hBest3 shows the most distinctive time-dependent current response, a large increase in whole-cell current developing on a time scale of many seconds. (*c*) As reported in Ref. [22], hBest1 and hBest2 differ by ~2-fold in their relative permeabilities to nitrate and chloride. At present, the physiologic significance of these differences in channel properties remains to be determined.

As noted under “Results,” the 61 amino acid substitutions in hBest1 reported to date in VMD patients cluster within the N-terminal domain (Figs. 1*C* and 8*A*). In genetic diseases that involve loss of protein stability or function, disease-associated missense mutations typically cluster in regions that are conserved in evolution (*e.g.* Ref. 40). By contrast, the reported bestrophin mutations show only modest colocalization with conserved positions (Fig. 1*C*). This pattern likely reflects the mechanism of dominance in VMD: coassembly of structurally intact mutant and wild type subunits to produce a defective channel (22). Thus the VMD mutations define a subset of positions that (*a*) are not critical for folding and multimeric assembly, and (*b*) control channel closure either via steric or allosteric mechanisms.

Bestrophins Have a Complex Transmembrane Topography

The hBest1 hydropathy profile (Fig. 8*A*), which is representative of the entire bestrophin family, reveals between four and six candidate membrane spanning domains (*labeled A–F* in Fig. 8). Transmembrane models of hBest1 with four or five transmembrane segments have been proposed previously (Fig. 8*C*, *model 2* (28) and *model 3* (30)). A survey of publicly available transmembrane prediction algorithms suggests that any of the four models shown at the *left* in Fig. 8*C* are plausible for hBest1: model 4, (41, 42; www.enzim.hu/hmmtop/html/document.html); models 2 and 4, (43; sosui.proteome.bio.tuat.ac.jp/sosuiframe0.html); model 2, (44; www.cbs.dtu.dk/~krogh/TMHMM); models 1 and 3, (45, 46; www.ch.embnet.org/software/TMPRED_form.html); and model 4, (47; cubic.bioc.columbia.edu/predictprotein).

The topography mapping presented here significantly constrains any models for bestrophin structure (Fig. 8*B*). TEVP cleavage indicates that the N and C termini face the cytosol, and it is also suggestive for a cytosolic localization of position 154 in the center of the N-terminal domain. Glycosylation insertion mutagenesis identifies three regions (60–63, 212–227, and 261–267) that face the extracellular space. The small size of the MTSET reagent relative to TEVP or the ER glycosyltransferase and the requirement that MTSET modification alters channel properties to reveal its covalent reaction make any topographic interpretation of the MTSET experiments potentially more complex. However, the extracellular region 212–227 defined by *N*-glycosylation encompasses residues 223 and 226, where MTSET modification alters channel properties. Similarly, extracellular region 60–63 defined by *N*-glycosylation is close to cysteine 69, the endogenous cysteine that is the target of MTSET modification. Finally, it is intriguing that the extended cluster of cysteine-substitution mutants that confer MTSET sensitivity reside along hydrophobic segment B, suggesting that at least one face of this segment is accessible to extracellular probes.

A working model that incorporates the topographical constraints described above is presented in Fig. 8*C* (*right*). Although the data are consistent with more complex topographies, this model is the most parsimonious. The model shows the predicted locations of hydrophobic segments A, B, D, E, and F, but we have indicated with a *question mark* the transmembrane assignment of hydrophobic segment D because the experimental data only roughly constrain this region. Similarly, a *vertical arrow* and *question mark* accompany hydrophobic segment E which, based on its hydrophobicity, is shown dipping into the bilayer region but which could instead reside entirely beyond the bilayer as predicted for the immediately flanking regions.

In mapping the transmembrane topography of hBest1 by *N*-glycosylation site insertion, we observed that wild type hBest1 carries no *N*-linked carbohydrate. Moreover, a comparison of other bestrophin sequences reveals no evidence for conserved Asn-*X*-Ser/Thr sequences, suggesting that this may be a general property of the bestrophin family. The absence of *N*-glycosylation in wild type hBest1 greatly facilitates the detection of the ~3-kDa electrophoretic mobility shift due to the addition of a single *N*-linked carbohydrate chain. Beyond its technical utility in this context, this finding sets the bestrophins apart from the majority of integral membrane proteins, which carry at least one site of *N*-glycosylation. *N*-Glycosylation is proposed to facilitate protein folding and assembly in the ER (48); for lysosomal proteins it plays an essential role in intracellular trafficking (49).

The systematic insertion of TEVP cleavage sites along a polypeptide chain is introduced here for the first time as a method for mapping transmembrane topography. This method should be generally applicable to other membrane proteins. As mammalian cells tolerate active TEVP in the cytosol (50), presumably because of its high substrate specificity, one potential extension of these experiments would be to carry out the cleavage in living cells by coexpressing the target protein with TEVP, as demonstrated by Faber *et al.* (51) in a study of yeast peroxisomal protein topography. As seen for insertion of *N*-glycosylation sites, the efficiency of TEVP cleavage is highly dependent on the location and/or accessibility of the inserted sites. To make the efficiency of TEVP cleavage less dependent on location, it might be possible to carry out the insertional mutagenesis with a small autonomously folding protein domain that includes an efficiently cleaved TEVP site.

Allosteric Activation of h Best1

One unexpected outcome of the cysteine-substitution experiments was the finding that MTSET modification of positions 79, 80, 83, 87, and 90 within the second predicted transmembrane segment produces a sustained increase in whole-cell current. MTSET-dependent activation presumably occurs via an allosteric mechanism, and therefore these findings implicate this region in the modulation of channel opening. By contrast, MTSET-dependent inhibition of

whole-cell current, as observed with modification of the endogenous cysteine at position 69 or cysteines substituted at positions 78 and 226, can be explained either by steric block of the pore or via an indirect (allosteric) mechanism.

The diverse and rapid effects of MTSET modification on current responses of cells transfected with different cysteine-substitution mutants of hBest1, together with the diverse current responses exhibited by cells transfected with different bestrophin family members, lend strong support to the general conclusion that the bestrophins function directly as anion channels. A challenge for the future will be to relate the characteristics of the isolated recombinant bestrophins to their roles in the intact organism.

Acknowledgments

We thank Dan Leahy for providing the hGH-HER3 EC domain plasmid; Robert Molday for mAb RIM3F4; Jennifer Doudna for the TEVP expression plasmid; Thomas Jentsch for the CLC-0 expression plasmid; Jonathan Pevsner for advice on sequence analysis; and Tsung-Yu Chen for helpful comments on the manuscript.

REFERENCES

1. Jentsch TJ, Gunther W. BioEssays 1997;19:117–126. [PubMed: 9046241]
2. George AL, Bianchi L, Link EM, Vanoye CG. Curr. Biol 2001;11:R620–R628. [PubMed: 11516971]
3. Hille, B. Ion Channels of Excitable Membranes. Sunderland, MA: Sinauer Associates, Inc.; 2001.
4. Gunther W, Luchow A, Cluzead F, Vandewalle A, Jentsch TJ. Proc. Natl. Acad. Sci. U. S. A 1998;95:8075–8080. [PubMed: 9653142]
5. Iyer R, Iverson TM, Accardi A, Miller C. Nature 2002;419:715–718. [PubMed: 12384697]
6. Dutzler R, Campbell EB, Cadene M, Chait BT, MacKinnon R. Nature 2002;415:287–294. [PubMed: 11796999]
7. Wisden W, Seeburg PH. Curr. Opin. Neurobiol 1992;2:263–269. [PubMed: 1379501]
8. Betz H, Kuhse J, Schmieden V, Laube B, Kirsch J, Harvey RJ. Ann. N. Y. Acad. Sci 1999;868:667–676. [PubMed: 10414351]
9. Zielenski J, Tsui LC. Annu. Rev. Genet 1995;29:777–807. [PubMed: 8825494]
10. Cunningham SA, Awayda MS, Bubien JK, Ismailov II, Arrate MP, Berdiev BK, Benos DJ, Fuller CM. J. Biol. Chem 1995;270:31016–31026. [PubMed: 8537359]
11. Gandhi R, Elble RC, Gruber AD, Schreur KD, Ji HL, Fuller CM, Pauli BU. J. Biol. Chem 1998;273:32096–32101. [PubMed: 9822685]
12. Marquardt A, Stohr H, Passmore LA, Kramer F, Rivera A, Weber BH. Hum. Mol. Genet 1998;7:1517–1525. [PubMed: 9700209]
13. Petrukhin K, Koisti MJ, Bakall B, Li W, Xie G, Marknell T, Sandgren O, Forsman K, Holmgren G, Andreasson S, Vujic M, Bergen AA, McGarty-Dugan V, Figueroa D, Austin CP, Metzker ML, Caskey CT, Wadelius C. Nat. Genet 1998;19:241–247. [PubMed: 9662395]
14. Francois J, De Rouck A, Fernandez-Sasso D. Arch. Ophthalmol 1967;77:727–733.
15. Deutman AF. Arch. Ophthalmol 1969;81:305–316. [PubMed: 5774285]
16. Mohler CW, Fine SL. Ophthalmology 1981;88:688–692. [PubMed: 7267039]
17. Frangieh GT, Green WR, Fine SL. Arch. Ophthalmol 1982;100:1115–1121. [PubMed: 7092655]
18. Weingeist TA, Kobrin JL, Watzke RC. Arch. Ophthalmol 1982;100:1108–1114. [PubMed: 7092654]
19. Steinberg RH, Linsenmeier RA, Griff ER. Prog. Retinal Res 1985;4:33–66.
20. Gallemore, RP.; Hughes, BA.; Miller, SS. The Retinal Pigment Epithelium. Marmor, MF.; Wolfensberger, TJ., editors. Oxford, UK: Oxford University Press; 1998. p. 175-198.
21. Marmorstein AD, Marmorstein LY, Rayborn M, Wang X, Hollyfield JG, Petrukhin K. Proc. Natl. Acad. Sci. U. S. A 2000;97:12758–12763. [PubMed: 11050159]
22. Sun H, Tsunenari T, Yau K-W, Nathans J. Proc. Natl. Acad Sci. U. S. A 2002;99:4008–4013. [PubMed: 11904445]
23. Nathans J, Thomas D, Hogness DS. Science 1986;232:193–202. [PubMed: 2937147]

24. Illing M, Molday LL, Molday RS. J. Biol. Chem 1997;272:10303–10310. [PubMed: 9092582]
25. Lucast LJ, Batey RT, Doudna JA. BioTechniques 2001;30:544–546. [PubMed: 11252791]
26. Leahy DJ, Dann CE, Longo P, Perman B, Ramyar KX. Protein Expression Purif 2000;20:500–506.
27. Stohr H, Marquardt A, Nanda I, Schmid M, Weber BH. Eur. J. Hum. Genet 2002;10:281–284. [PubMed: 12032738]
28. Bakall B, Marknell T, Ingvast S, Koisti MJ, Sandgren O, Li W, Bergen AA, Andreasson S, Rosenberg T, Petrukhin K, Wadelius C. Hum. Genet 1999;104:383–389. [PubMed: 10394929]
29. Lotery AJ, Munier FL, Fishman GA, Weleber RG, Jacobson SG, Affatigato LM, Nichols BE, Schorderet DF, Sheffield VC, Stone EM. Investig. Ophthalmol. Vis. Sci 2000;41:1291–1296. [PubMed: 10798642]
30. White K, Marquardt A, Weber BHF. Hum. Mutat 2000;15:301–308. [PubMed: 10737974]
31. Marchant D, Gogat K, Boutboul S, Pequignot M, Sternberg C, Dureau P, Roche O, Uteza Y, Hache JC, Puech B, Puech V, Dumur V, Mouillon M, Munier FL, Schorderet DF, Marsac C, Dufier JL, Abitbol M. Hum. Mutat 2001;17:235. [PubMed: 11241846]
32. Karlin A, Akabas MH. Methods Enzymol 1998;293:123–145. [PubMed: 9711606]
33. Zelenski NG, Rawson RB, Brown MS, Goldstein JL. J. Biol. Chem 1999;274:21973–21980. [PubMed: 10419520]
34. Carrington JC, Dougherty WG. Proc. Natl. Acad. Sci. U. S. A 1988;85:3391–3395. [PubMed: 3285343]
35. Popov M, Tam LY, Li J, Reithmeier RA. J. Biol. Chem 1997;272:18325–18332. [PubMed: 9218473]
36. Chang X-B, Hou Y-X, Jensen TJ, Riordan JR. J. Biol. Chem 1994;269:18572–18575. [PubMed: 7518437]
37. Turk E, Kerner CJ, Lostao MP, Wright EM. J. Biol. Chem 1996;271:1925–1934. [PubMed: 8567640]
38. Yellen G. Nature 2002;419:35–42. [PubMed: 12214225]
39. Marmorstein LY, McLaughlin PJ, Stanton JB, Yan L, Crabb JW, Marmorstein AD. J. Biol. Chem 2002;277:30591–30597. [PubMed: 12058047]
40. Macke JP, Davenport CM, Jacobson SG, Hennessey JC, Gonzalez-Fernandez F, Conway BP, Heckenlively J, Palmer R, Maumenee IH, Sieving P, Gouras P, Good W, Nathans J. Am. J. Hum. Genet 1993;53:80–89. [PubMed: 8317502]
41. Tusnady GE, Simon I. J. Mol. Biol 1998;283:489–506. [PubMed: 9769220]
42. Tusnady GE, Simon I. Bioinformatics 2001;17:849–850. [PubMed: 11590105]
43. Hirokawa T, Boon-Chieng S, Mitaku S. Bioinformatics 1998;14:378–379. [PubMed: 9632836]
44. Sonnhammer, ELL.; von Heijne, G.; Krogh, A. In: Glasgow, J.; Littlejohn, T.; Lathrop, FMR.; Sankoff, D.; Sensen, C., editors. Proceedings of the 6th International Conference on Intelligent Systems for Molecular Biology, Montreal, Quebec, Canada, June 28–July 1, 1998; Menlo Park, CA: AAAI Press; 1998. p. 175-182.
45. Hofmann K, Stoffel W. Comput. Appl. Biosci 1992;8:331–337. [PubMed: 1498688]
46. Hofmann K, Stoffel W. Biol. Chem. Hoppe-Seyler 1993;374:166.
47. Rost B, Fariselli P, Casadio R. Protein Sci 1996;5:1704–1718. [PubMed: 8844859]
48. Ellgaard L, Helenius A. Nat. Rev. Mol. Cell. Biol 2003;4:181–191. [PubMed: 12612637]
49. Ghosh P, Dahms NM, Kornfeld S. Nat. Rev. Mol. Cell. Biol 2003;4:202–212. [PubMed: 12612639]
50. Urabe M, Kume A, Takahashi T, Serizawa N, Tobita K, Ozawa K. Biochem. Biophys. Res. Commun 1999;266:92–96. [PubMed: 10581171]
51. Faber KN, Kram AM, Ehrmann M, Veenhuis M. J. Biol. Chem 2001;276:36501–36507. [PubMed: 11443138]
52. Kyte J, Doolittle RF. J. Mol. Biol 1982;157:105–132. [PubMed: 7108955]

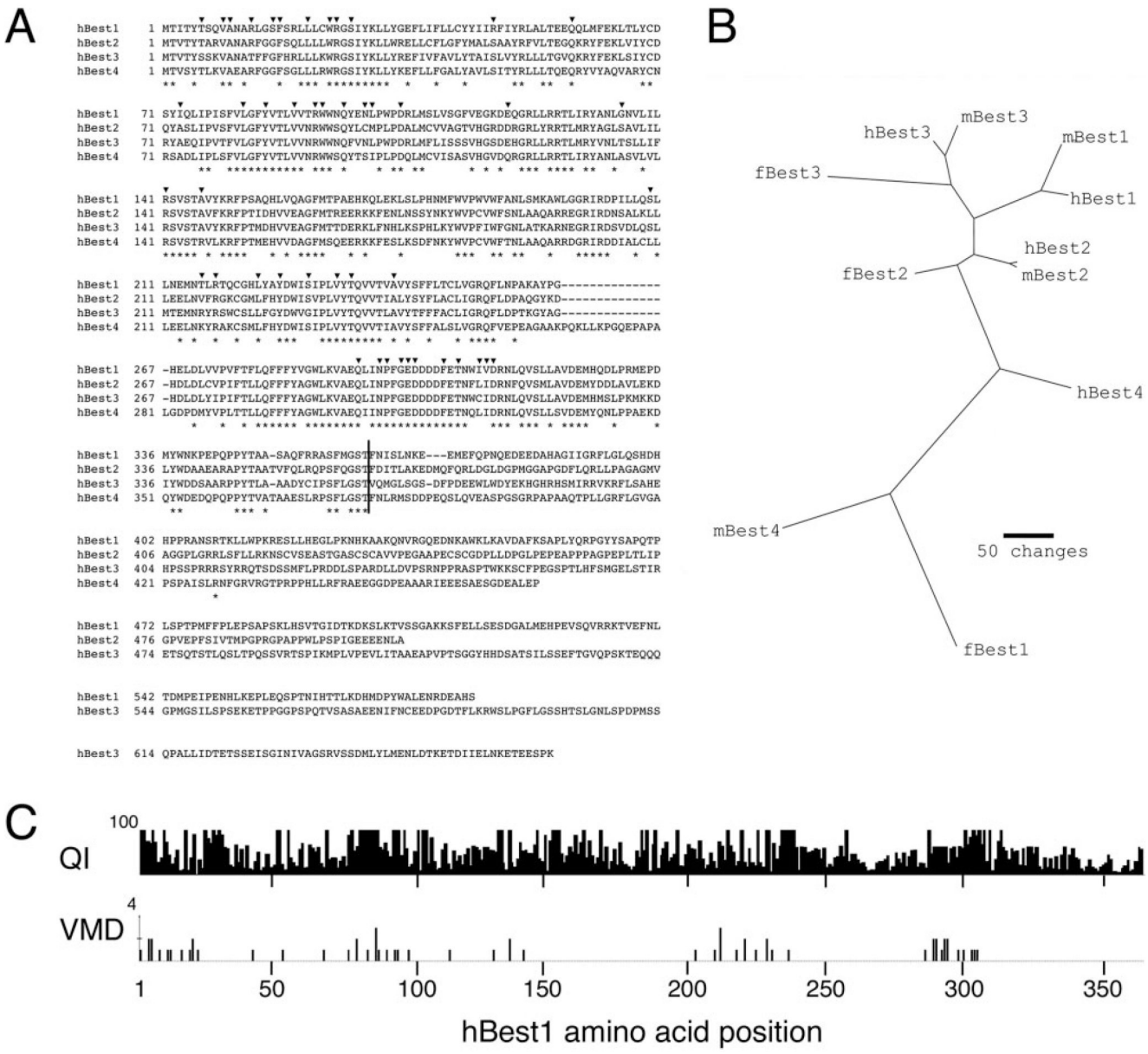

FIG. 1. Sequence analysis of bestrophin family members

A, amino acid sequences of hBest1-hBest4 deduced from cloned cDNA. An *arrowhead above* the aligned sequences indicates the locations of VMD-associated missense mutations. An *asterisk* below the aligned sequences indicates those residues that are identical among all human and mouse bestrophins. *B*, unrooted dendrogram in which the line lengths represent the degree of amino sequence divergence within the conserved ~360 N-terminal amino acids for bestrophin family members from human (hBest), mouse (mBest), and pufferfish (fBest), and their presumptive ancestral sequences at the nodal points. For each bestrophin, the N-terminal domain was considered to end at the position that aligns with amino acid 364 in hBest1 (*vertical line* in *A*). *C*, analysis of the N-terminal domain of bestrophin. *Top*, amino acid sequence conservation among all human, mouse, pufferfish, and mosquito bestrophins, and *Drosophila* bestrophins 1 and 2 scored with a PAM350 matrix with an open gap penalty of 5 using ClustalX software; the *vertical axis* shows the quality score (*QI*; range, 0–100), higher

values of which indicate greater conservation. *Bottom*, histogram showing the locations of 61 amino acid substitution mutations in hBest1 reported in patients with juvenile or adult onset VMD. The *vertical axis* shows the number of different amino acid substitutions at each position along the polypeptide. For *C*, the amino acid numbering refers to hBest1, and therefore gaps in the hBest1 sequence were omitted from the alignments used to generate the *upper plot*.

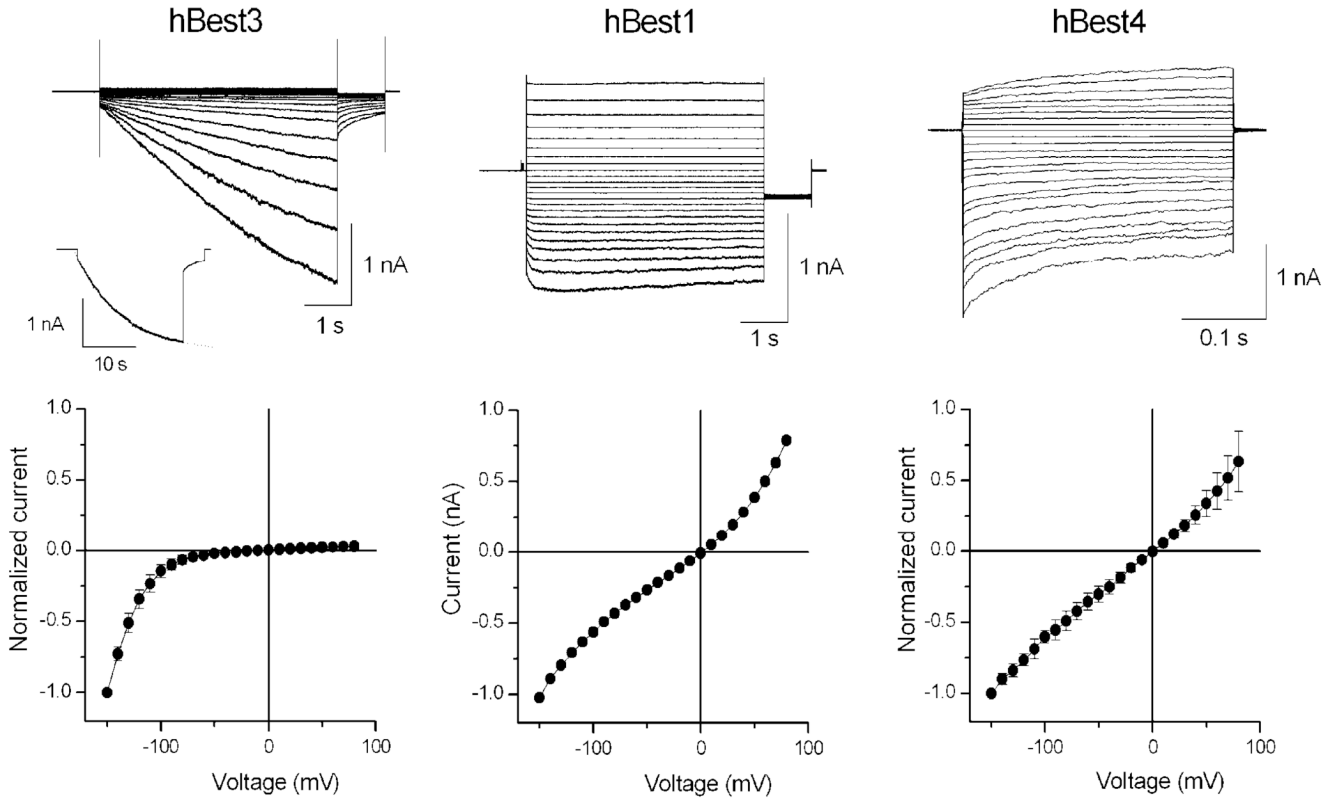

FIG. 2. Whole-cell currents and current-voltage relationships from 293 cells transiently transfected with human bestrophin cDNAs

Left, hBest3; *center*, hBest1; *right*, hBest4. For hBest1 and hBest3, whole-cell currents were measured in response to 5-s steps to variable test voltages, followed by a 1-s step to −50 mV. Voltage steps were in 10-mV intervals from −150 to +80 mV starting from a holding potential of 0 mV. For hBest3, the *inset* shows the whole-cell current response to a 20-s step to −150 mV, followed by a 4-s step to −50 mV. For hBest4, whole-cell currents were measured in response to voltage steps of 320 ms starting from a holding potential of 0 mV, with voltage steps in 10-mV intervals from −150 to +80 mV. The I-V curves for each bestrophin were obtained from five cells (hBest3), four cells (hBest4), or one cell (hBest1) and were normalized to a value of −1.0 at −150 mV before averaging. Current amplitudes at the end of the variable voltage steps were used for the I-V plots. *Error bars* indicate standard deviations. Recordings were performed with standard extracellular and pipette solutions.

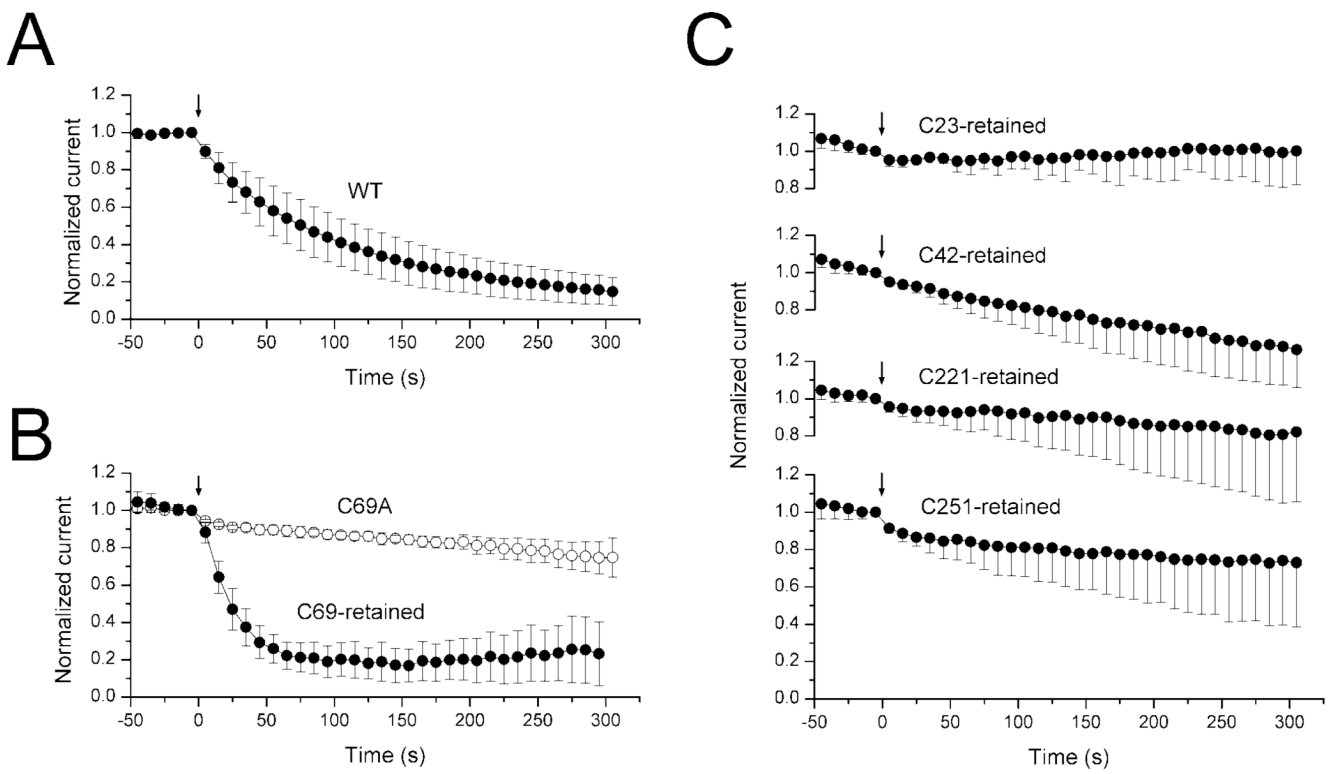

FIG. 3. Cysteine 69 is the principal target of current inactivation by the sulfhydryl-specific reagent MTSET

293 cells were transiently transfected with wild type (*WT*) hBest1 (*A*), hBest1 C69A (*upper curve*) or hBest1 in which Cys-69 is the only cysteine present (C69-retained; *lower curve*) (*B*), or hBest1 mutants in which Cys-23, Cys-42, Cys-221, or Cys-251 are the only cysteines present (*C*). In the hBest1 mutants that retain a single cysteine, each of the other 4 cysteines has been mutated to alanine. Each panel shows the average current recorded at +80 mV ± S.D. At 1-s intervals, the cells were stepped for 150 ms from a holding potential of 0 mV to test potentials of −120, −80, −40, 0, +40, and +80 mV; the entire cycle was repeated every 10 s for the duration of the experiment. Currents are normalized to 1.0 at the fifth time point, immediately prior to addition of 1 mM MTSET at time 0 (*downward arrow*). Mean current amplitudes at + 80 mV recorded immediately before MTSET addition were: 1028 ± 217 pA (*n* = 7; wild type); 610 ± 399 pA (*n* = 5; C69A); 605 ± 374 pA (*n* = 5; C69-retained); 462 ± 407 pA (*n* = 4; C23-retained); 494 ± 236 pA (*n* = 6; C42-retained); 960 ± 843 pA (*n* = 5; C221-retained); and 623 ± 508 pA (*n* = 6; C251-retained).

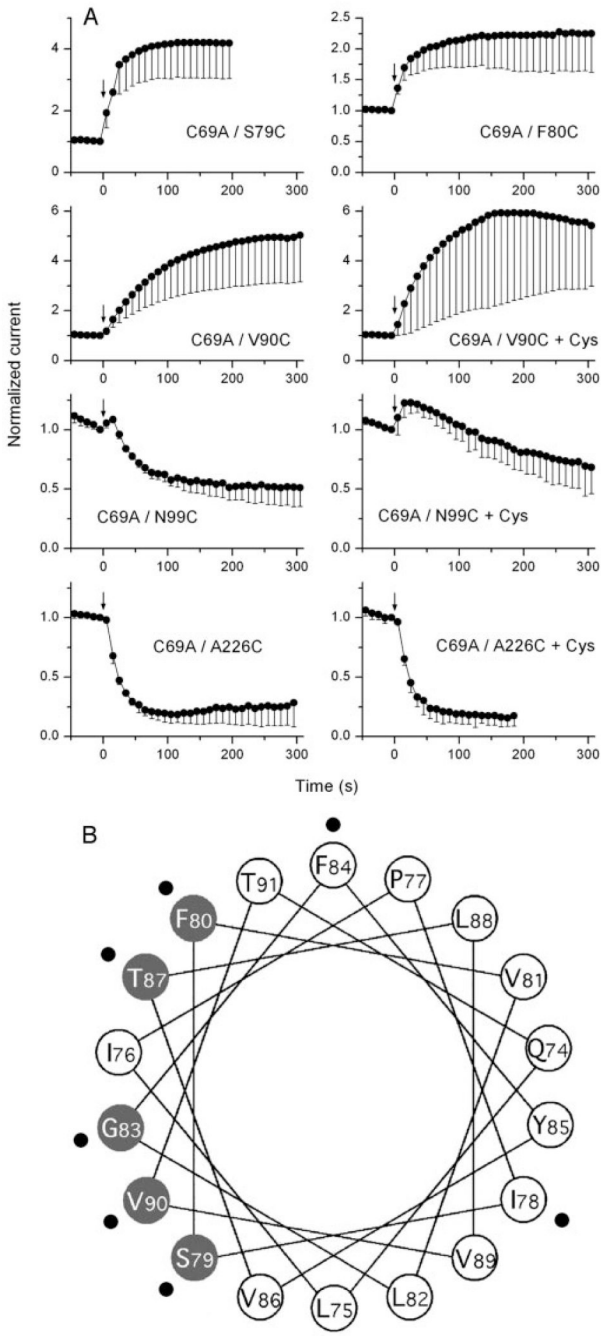

FIG. 4. Activation and inactivation of whole-cell currents by MTSET modification of cysteine-substitution mutants

A, each cysteine-substitution mutant was constructed on the C69A background to eliminate the principal endogenous target for MTSET-dependent inactivation. *Left*, whole-cell currents were recorded and analyzed as described for Fig. 3. Cells expressing C69A/S79C and C69A/F80C were exposed to 20 and 100 μM MTSET, respectively, as their reaction with 1mM MTSET was too rapid to be resolved accurately; all other cells were exposed to 1 mM MTSET. For C69A/V90C, C69A/N99C, and C69A/A226C external MTSET was applied with either standard pipette solution (*left panels*) or with 20 mM cysteine in the pipette (*right panels*). Activation of C69A/V90C whole-cell current and inactivation of C69A/A226C whole-cell

current by MTSET was unaffected by intracellular cysteine, whereas the rapid partial inactivation of C69A/N99C whole-cell current by MTSET was abolished by intracellular cysteine. Mean current amplitudes at + 80 mV recorded immediately before MTSET addition were: 588 ± 529 pA (*n* = 3; C69A/S79C); 323 ± 143 pA (*n* = 4; C69A/F80C); 2490 ± 1047 pA (*n* = 3; C69A/T87C); 841 ± 716 pA (*n* = 6; C69A/V90C); 605 ± 307 pA (*n* = 3; C69A/V90C with 20 mM cysteine); 617 ± 164 pA (*n* = 4; C69A/N95C); 341 ± 304 pA (*n* = 4; C69A/N99C); 541 ± 597 pA (*n* = 4; C69A/N99C with 20 mM cysteine); 834 ± 424 pA (*n* = 4; C69A/A226C); 347 ± 192 pA (*n* = 3; C69A/A226C with 20 mM cysteine). *B*, helical wheel representation of residues 74–91 showing those locations where cysteine substitution and externally applied MTSET confers any measurable effect (*small black dots*) or a sustained activation (*filled symbols*).

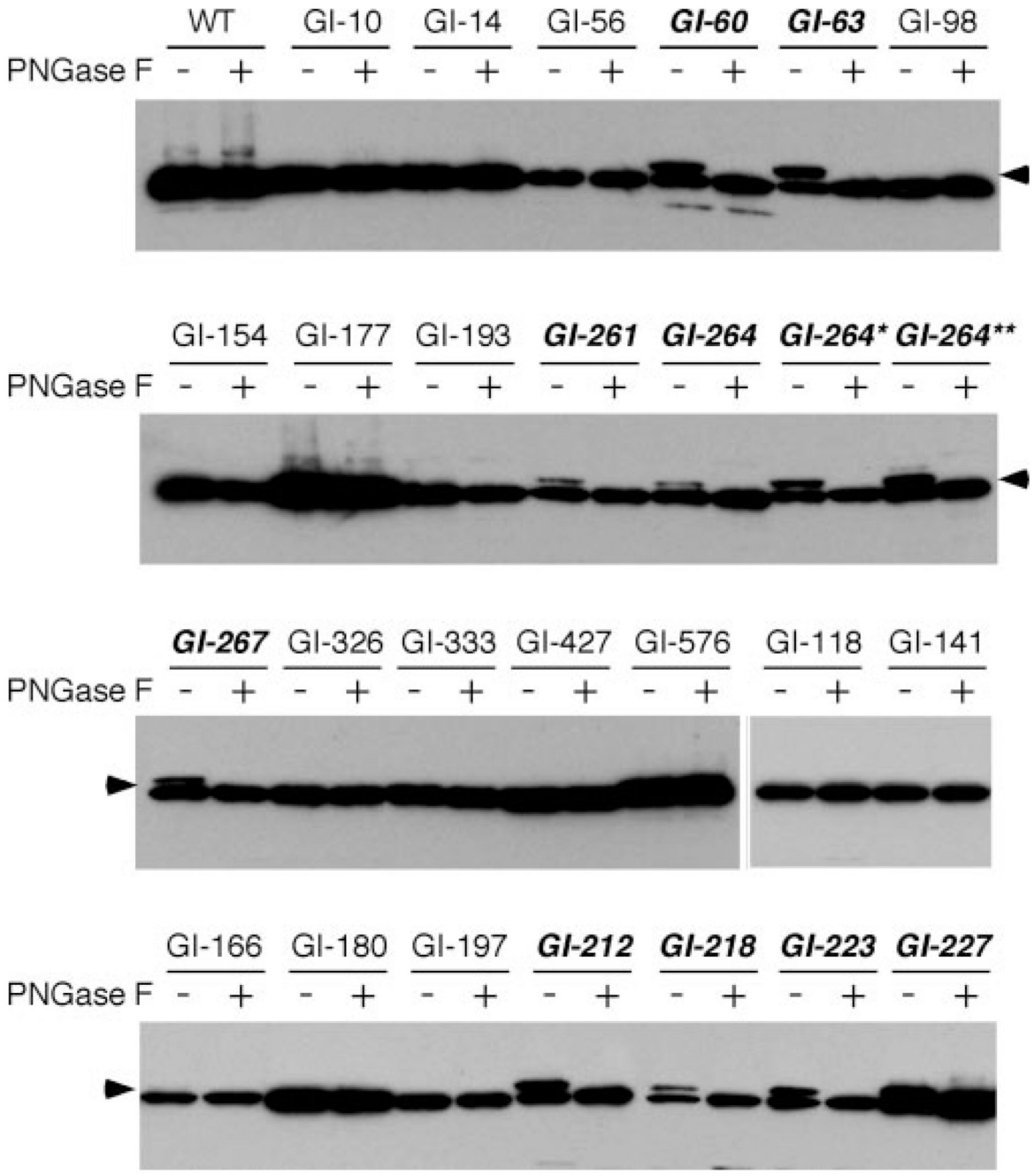

FIG. 5. Mapping the transmembrane topography of hBest1 by insertion of *N*-linked glycosylation sites

293 cells were transfected with the indicated hBest1 mutants tagged at their extreme C termini with the Rim3F4 epitope. Each mutant carries the sequence GGNATGG inserted in-frame after the indicated codon, except for the two mutants that carry SGSGNATGSGS and GGNATNATGG after position 264, indicated as *GI-264** and *GI-264***, respectively. Cell lysates were incubated with or without peptide:*N*-glycosidase F (*PN-Gase F*) and analyzed by immunoblotting with mAb Rim3F4. Addition of a single *N*-linked oligosaccharide produces a band of lower mobility corresponding to an increase in molecular mass of ~3 kDa (*arrow*); mutants that were *N*-glycosylated are indicated in *boldface italics*. A shorter exposure shows

a single band at the wild type MW for GI-177 and a doublet for mutant GI-227. The *upper two panels*, and the *left panel on the 3rd line* show wild type hBest1 and the first set of 18 mutants (GI-10 to GI-576); the remaining *two panels* show the second set of 9 mutants (GI-118 to GI-227).

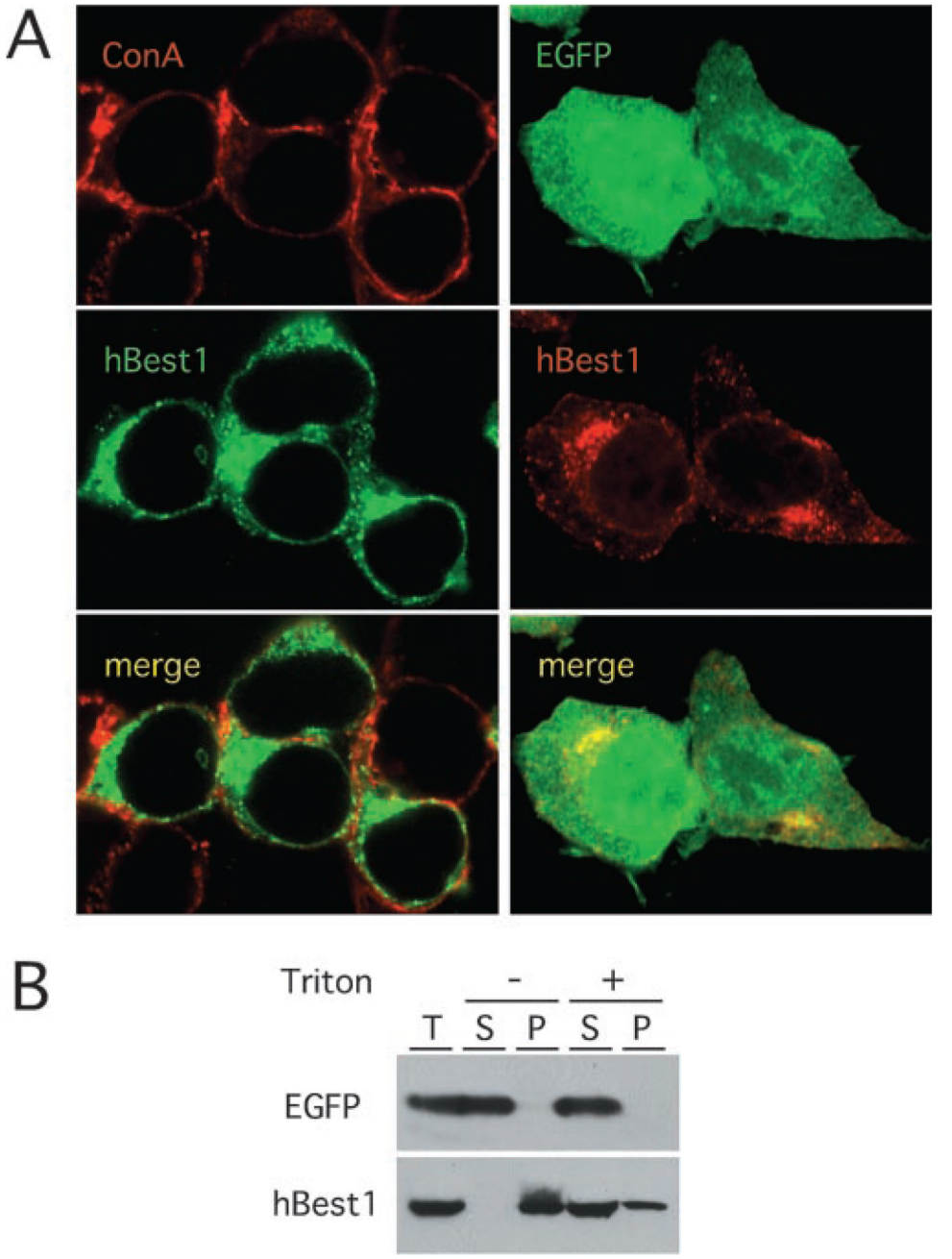

FIG. 6. Membrane association and subcellular localization of hBest1 in transfected 293 cells

A, *left panels*, immunolocalization of Rim3F4-tagged hBest1 following plasma membrane labeling of intact cells with concanavalin A. *Right panels*, immunolocalization of Rim3F4-tagged hBest1 and EGFP. The vast majority of the hBest1 protein accumulates in cytosolic vesicles; EGFP accumulates in both the nucleus and the cytosol. *B*, centrifugation of cellular homogenates at 25,000 × *g* for 30 min at 4 °C in the presence or absence of 1% Triton X-100. In the absence of detergent hBest1 is found in the membrane and cytoskeletal pellet. In the presence of Triton X-100 the majority of the hBest1 is solubilized. EGFP is soluble independent of detergent addition. *T*, total; *S*, supernatant; *P*, pellet.

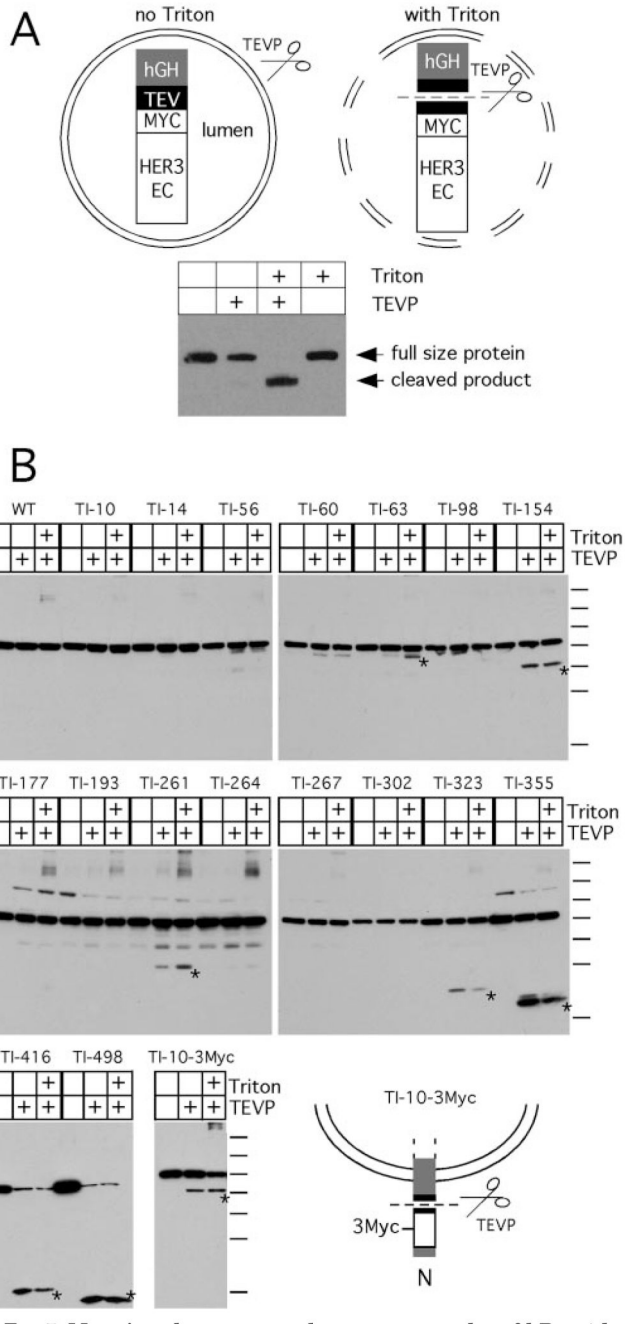

FIG. 7. Mapping the transmembrane topography of hBest1 by insertion of TEVP cleavage sites

A, control experiment in which an efficiently secreted hGH-TEV-myc-HER3EC fusion protein was expressed in transiently transfected 293 cells, and cell homogenates were subject to TEVP cleavage in the presence or absence of 1% Triton X-100. Immunoblotting with an anti-Myc mAb reveals cleavage at the TEVP site and release of the C-terminal myc-HER3EC fragment only in the presence of TEVP and detergent. The diagram illustrates the exclusion of added TEVP (*scissors*) from the interior of an intact membrane vesicle (*left*) and the access of TEVP to the vesicle interior in the presence of detergent (*right*). The vesicle lumen is topologically equivalent to the outside of the cell. *B*, TEVP cleavage of the indicated hBest1 mutants carrying a TEVP site insertion. Each mutant is tagged at the extreme C terminus with the Rim3F4

epitope, and proteins were visualized by immunoblotting with mAb Rim3F4. In the *1st 5 panels*, each mutant hBest1 carries the sequence GGENLYFQGGG inserted inframe after the indicated codon. The TI-10–3Myc mutant (*lower right autoradiogram*) carries an additional insertion of 3 Myc epitopes N-terminal to the TEVP cleavage site. The cleavage of this mutant by TEVP (*scissors*) is shown schematically at *the lower right*. A part of a membrane bilayer (*double lines*) separates the lumen (*upper area*) from the cytosol (*lower area*). Cleavage occurs on the cytosolic face of the membrane. *N*, N terminus; *3Myc*, triple Myc epitope tag. For each mutant, the molecular mass of the C-terminal fragment released by TEVP cleavage (*asterisk*) is determined by the point of insertion. *Bars* indicate molecular mass standards (from *top* to *bottom*) of 173, 111, 80, 61, 49, 36, and 25 kDa.

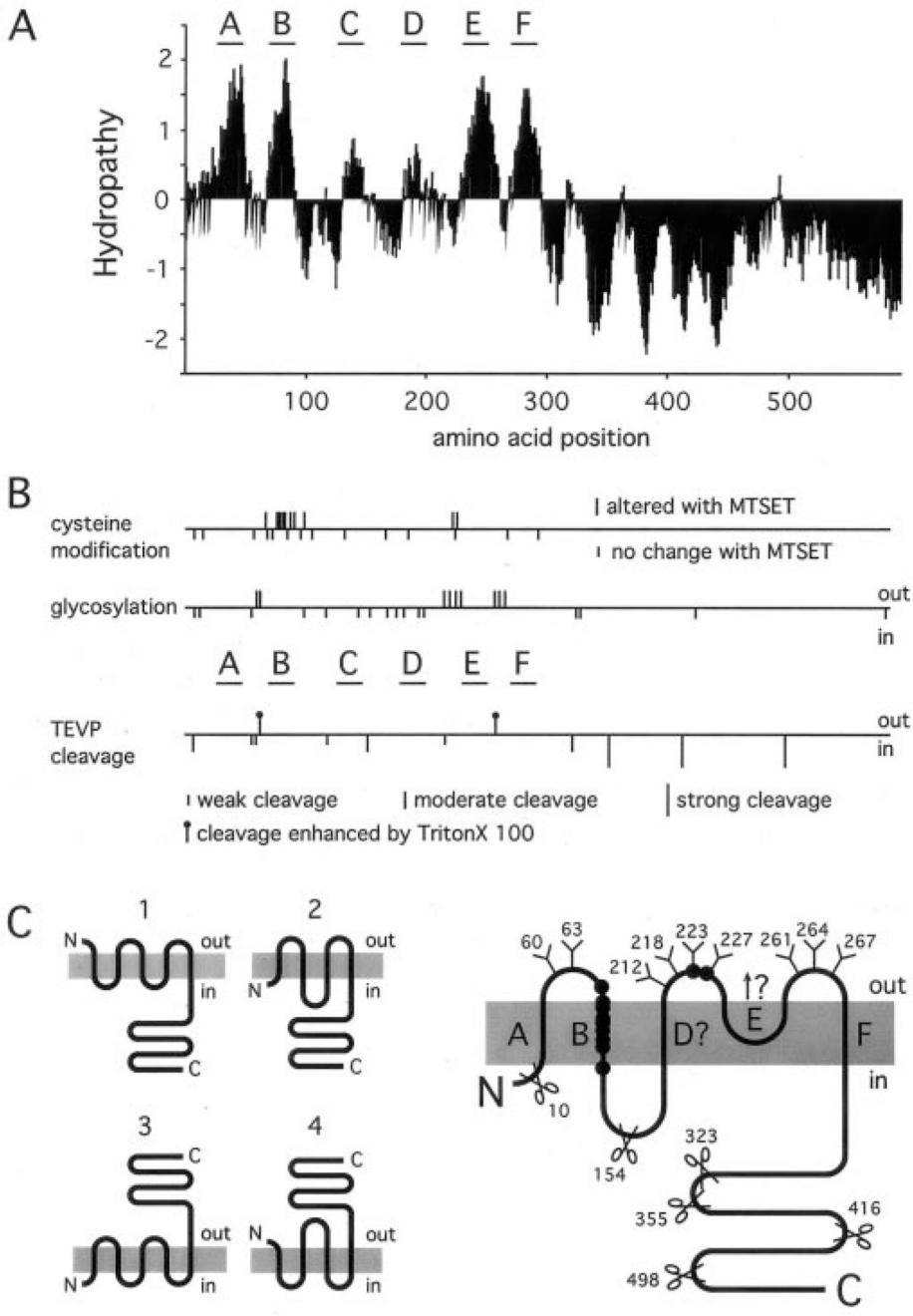

FIG. 8. Summary of structural and functional characteristics of hBest1

A, hydropathy profile calculated according to Kyte and Doolittle (52) with a window size of 19 residues. Increasing hydropathy is upward, and the six potential transmembrane segments are indicated by *horizontal bars* and *lettered A–F*. *B*, summary of hBest1 modifications. *Top*, MTSET modification of endogenous and introduced cysteines. Endogenous cysteine 69 and cysteine substitutions at positions 78, 79, 80, 83, 84, 87, 90, 99, 223, and 226 showed clear alterations in membrane current following exposure to MTSET; these positions are represented by *bars above the horizontal line*. Cysteine substitutions at positions 12, 16, 60, 71, 74, 86, 95, 108, 133, 169, 185, 225, 231, 268, and 293 produced whole-cell currents that were unaffected or minimally affected by exposure to MTSET; these are represented by *bars below the*

horizontal line. Cysteine substitutions that produced little or no measurable whole-cell current are not shown. *Center*, *N*-glycosylation site insertions. Insertions after positions 60, 63, 212, 218, 223, 227, 261, 264, and 267 were glycosylated and are therefore presumed to face the vesicle lumen, topologically equivalent to the outside of the cell; these are represented by *bars above the horizontal line*. Insertions after positions 10, 14, 56, 98, 154, 166, 177, 180, 193, 197, 326, 333, 427, and 576 were not glycosylated and are represented by *shorter bars below the horizontal line. Bottom*, TEVP cleavage site insertions. Insertions after positions 10, 154, 323, 355, 416, and 498 showed moderate or strong TEVP cleavage in the absence of added detergent and are therefore presumed to face the cytosol; they are represented by *bars below the horizontal line*, with *bar height* correlating with cleavage efficiency. Insertions after positions 63 and 261 showed enhanced TEVP cleavage in the presence of added detergent and are therefore presumed to face the vesicle lumen; these are represented by *bars* with *circles above the horizontal line*. Insertions that show very weak cleavage are represented by the *smallest bars* (positions 56, 60, 118, and 218) and were not incorporated into the transmembrane topography model. *C*, comparison of five models of hBest1 transmembrane topography. The four models on the *left* represent the most favored predictions based only on the hydropathy profile (see “Discussion”). The fifth model (*right*) accounts for the experimental data presented here. It is decorated with the locations of informative insertions of glycosylation sites (schematic sugar chains on the outer face of the protein), TEVP cleavage sites (scissors on the inner face of the protein), and the sites of cysteine modification by MTSET (*solid circles*).

TABLE I

Percent amino acid identity among human and murine bestrophins, divided into N- and C-terminal domains

Comparisons among orthologues are shown in boldface. The division between N- and C-terminal domains corresponds to position 364 in hBest1. Mouse bestrophin amino acid sequences are derived from the annotated mouse genome sequence (NCBI).

	Percent amino acid identity in the N-terminal domain						
	hBest1	**hBest2**	**hBest3**	**hBest4**	**mBest1**	**mBest2**	**mBest3**
hBest2	63						
hbest3	65	66					
hBest4	56	63	59				
mBest1	**82**	60	63	56			
mbest2	64	**95**	67	63	60		
mbest3	61	63	**93**	59	60	64	
mbest4	45	51	45	**69**	44	51	43
	Percent amino acid identity in the C-terminal domain						
	hBest1	hBest2	hBest3	hBest4	mBest1	mBest2	mBest3
hBest2	19						
hBest3	9	8					
hbest4	6	10	10				
mBest1	**36**	19	9	9			
mBest2	18	**74**	8	13	19		
mbest3	8	8	**56**	9	8	8	
mbest4	4	7	7	**34**	5	6	7

J Biol Chem. Author manuscript; available in PMC 2010 June 15.